Tandem internal models execute motor learning in the cerebellum

Takeru Honda[a,b,c,d,1], Soichi Nagao[b,c,e], Yuji Hashimoto[b], Kinya Ishikawa[b], Takanori Yokota[b], Hidehiro Mizusawa[b,d], and Masao Ito[f,1]

[a]Motor Disorders Project, Tokyo Metropolitan Institute of Medical Science, Setagaya-ku, 156-8506 Tokyo, Japan; [b]Department of Neurology and Neurological Science, Graduate School, Tokyo Medical and Dental University, Bunkyo-ku, 113-8510 Tokyo, Japan; [c]Laboratory for Motor Learning Control, RIKEN Brain Science Institute, Wako, 351-0198 Saitama, Japan; [d]National Center Hospital, National Center of Neurology and Psychiatry, Kodaira, 187-8551 Tokyo, Japan; [e]Laboratory for Integrative Brain Function, Nozomi Hospital, Kitaadachi-gun, Saitama 362-0806, Japan; and [f]Senior Advisor's Office, RIKEN Brain Science Institute, Wako, 351-0198 Saitama, Japan

Contributed by Masao Ito, May 26, 2018 (sent for review October 11, 2017; reviewed by Paul Dean and Stefan Pulst)

In performing skillful movement, humans use predictions from internal models formed by repetition learning. However, the computational organization of internal models in the brain remains unknown. Here, we demonstrate that a computational architecture employing a tandem configuration of forward and inverse internal models enables efficient motor learning in the cerebellum. The model predicted learning adaptations observed in hand-reaching experiments in humans wearing a prism lens and explained the kinetic components of these behavioral adaptations. The tandem system also predicted a form of subliminal motor learning that was experimentally validated after training intentional misses of hand targets. Patients with cerebellar degeneration disease showed behavioral impairments consistent with tandemly arranged internal models. These findings validate computational tandemization of internal models in motor control and its potential uses in more complex forms of learning and cognition.

motor control | forward model | inverse model | cerebellar degeneration | prism adaptation

In brain-based learning systems, internal models are fundamental for the regulation of behavioral repertoire, and their impairment can be linked to neurological diseases. In the cerebellum, two types of internal models, forward and inverse, have been proposed (for review, see refs. 1–3); forward models predict the sensory consequences of a performed movement (*SI Appendix*, Fig. S1*A*), whereas inverse models predict the motor commands that generate an appropriate sensory consequence (*SI Appendix*, Fig. S1*B*). These internal models are equipped with synaptic learning mechanisms to form, reform, and update them daily (4). In motor learning, the two types of internal model may operate independently of each other or under combinatorial interactions (e.g., ref. 5). However, evidence for such combinatorial interactions remains meager; there are few concrete cases of combinatorial motor learning for which both computational principles and behavioral data have been provided (e.g., ref. 6).

Hand reaching is a movement that can be evoked reflexively by a stimulus such as the appearance of a light spot, but its voluntary nature is evident because we can stop its execution at will. When repeated under prism lens conditions, hand-reaching movements show marked adaptation. In our previous test of prism adaptation, we identified two types of cerebellar patients (7). Patients of the first type were unable to adapt to the prism at all, as described by Martin et al. (8). Those of the second type, although they adapted to the prism, were unable to memorize prismatic deviations after removal of the prism (7). These observations suggest that there are multiple forms of deterioration of the internal models in the cerebellum but do not clarify their structure.

In this study, we developed a computational model composed of a hybrid of forward and inverse models (*SI Appendix*, Fig. S1*C*). In this model, a forward model, a controller, and an inverse model are connected in parallel, but their learning operations occur serially or in tandem; in this sense we call it a "tandem model." Using this tandem model, we analyzed prism adaptation of hand reaching. We quantitatively defined the gains and parameters of the tandem model and validated its existence and functional significance in motor learning. Furthermore, independent evidence for the cooperation between the forward and inverse models in cerebellar learning was shown by the selective impairment of model components in patients with cerebellar degeneration disease.

Results

Ten healthy subjects (*SI Appendix*, Table S1) and 10 cerebellar disease patients (*SI Appendix*, Table S2) were tested. In each trial, a subject was instructed to reach for a target appearing on the touchscreen with his/her right index finger under various visual feedback conditions and instructions (Fig. 1 *A* and *B*). To induce adaptation, the subject repeated hand reaching while viewing the target through a Fresnel prism plate mounted on the goggles.

The effect of prism adaptation was examined by plotting horizontal deviations of the index finger's positions from the target spot in the ordinate as a function of t in the abscissa (Figs. 1–3 and *SI Appendix*, Fig. S2). Note that t is defined as a discrete trial number.

Psychophysical Experiments Revealed Adaptation and Hidden Learning. Three types of task were used to test these subjects. In the aimed offline-feedback (AOF) task paradigm the target spot that disappeared after the initiation of hand reaching appeared

Significance

The formation and dissolution of internal models of the human body occur in the cerebellum, and their logical organization is essential for normal motor learning. Here, we propose that the two known types of internal models, forward and inverse, are combined into one tandem model. We analyzed human motor learning, theoretically and experimentally, in a prism-adaptation hand-reaching task. Remarkably, the behavioral analyses and computational modeling converged to support the existence of a tandem model and reveal its unique features in cerebellum-based motor learning. For example, intentional misreaching induced covert learning in the tandem model. Finally, the tandem model was used to index the nature and degree of cerebellar damage in patients.

Author contributions: T.H., S.N., and M.I. designed research; T.H., Y.H., K.I., T.Y., and H.M. performed research; T.H. contributed new reagents/analytic tools; T.H. analyzed data; T.H. and M.I. wrote the paper; T.H. conceptualized the model and developed the theories; K.I., T.Y., and H.M. managed healthy subjects and cerebellar patients; and M.I. conceptualized the model.

Reviewers: P.D., University of Sheffield; and S.P., University of Utah.

The authors declare no conflict of interest.

[1]To whom correspondence may be addressed. Email: takeru@brain.riken.jp or masao@brain.riken.jp.

This article contains supporting information online at www.pnas.org/lookup/suppl/doi:10.1073/pnas.1716489115/-/DCSupplemental.

Published online June 25, 2018.

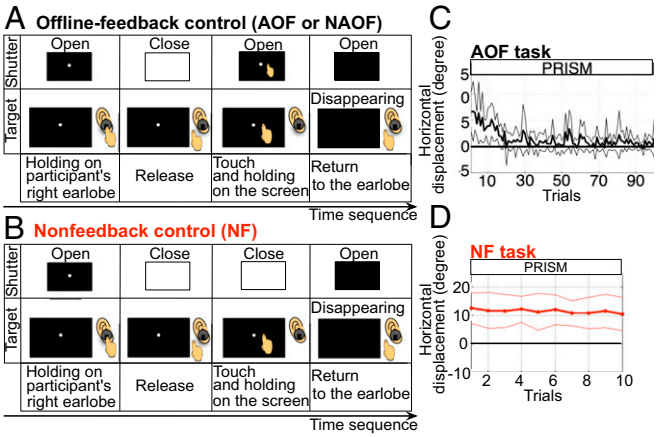

Fig. 1. Stages of hand reaching and operations in the prism-adaptation experiment. (*A*) Experimental procedures of the AOF or NAOF tasks. (*B*) Experimental procedures of the NF task. (*C*) Prism adaptation in healthy subjects ($n = 5$) during the AOF task. The thick and thin lines represent the mean and mean ± SD, respectively. (*D*) There was no adaptation in healthy subjects wearing a Fresnel prism plate during the NF task ($n = 10$).

again as soon as the index finger hit the touchscreen, and the shutter on the goggles opened briefly, for 0.1 s (Fig. 1*A*). The available offline feedback enabled the subject to confirm the outcome of the just-performed hand reaching and to determine how to hit more closely to the target in subsequent trials. When the prism plate produced a displacement of the target spot 25° to the right, the hit spots were initially displaced to the right; however, the degree of displacement decreased rapidly as the subject adapted during repeated trials (Fig. 1*C*).

The nonfeedback (NF) task was another paradigm used in the test in which the subject was deprived of all visual feedback, including the offline feedback (Fig. 1*B*). After the target spot was viewed through the 25°-displacing Fresnel prism plate, the hit points markedly deviated from the target (11.5 ± 5.6°) and remained deviated in all the repeated NF task trials. Thus, no adaptation occurred during the NF task ($P > 0.05$, one-way ANOVA) (Fig. 1*D*).

Repeated alternations between 10 trials of the AOF task and five trials of the NF task, for a total of 210 trials, revealed the dual nature of motor adaptation. The degree of horizontal displacement induced during the AOF task decreased rapidly (fast adaptation), as shown in the average of five healthy subjects (black dots in Fig. 2*A*) and in a single healthy subject (*SI Appendix*, Fig. S2*E*). On the other hand, the NF task trials revealed a significantly less rapid adaptation (slow adaptation), as shown in the average of the five healthy subjects (red dots in Fig. 2*A*) and in a single case (*SI Appendix*, Fig. S2*E*). The decay to 36.8% of the horizontal displacements of the initial trial took 37 trials in the fast adaptation and 113 trials in the slow adaptation ($P < 0.05$, Mann–Whitney *U* test) (Fig. 2*B*). Because the NF task induced no adaptation by itself (Fig. 1*D*), results of the NF task trials in Fig. 2*A* could be excluded to obtain the net fast and slow adaptations (Fig. 2*C*) ($P < 0.05$, Mann–Whitney *U* test in Fig. 2*D*). Results of the initial 10 trials of the NF task in Fig. 2*A* (in the BEFORE block) show the zero baseline (broken lines in Fig. 2 *A* and *C*) for the fast and slow adaptations.

Interestingly, we found that the subsequent psychophysical instruction, i.e., the nonaimed offline-feedback (NAOF) task, also blocked prism adaptation effectively. In this third paradigm, the subject was instructed to intentionally ignore the results of the preceding trial of hand reaching; therefore, the offline feedback should have no effect on prism adaptation (Fig. 1*A*).

Alternating performance of the NAOF and NF tasks resulted in large prism-induced horizontal displacements of hit points, which remained unchanged (from 16.5 ± 2.5° in the BEFORE block to 17.1 ± 2.2° in the TEST block in Fig. 2*E*; $P > 0.05$, Mann–Whitney *U* test). There is no sign of adaptation occurring during the AOF task (from 13.9 ± 1.8° in the BEFORE block to 0.5 ± 1.0° in the TEST block in Fig. 2*A*; $P < 0.01$, Mann–Whitney *U* test) (Compare also test blocks in Fig. 2 *A* and *E*, as shown in Fig. 2*F*; $P < 0.01$, Mann–Whitney *U* test).

A surprising observation was that immediately after 30 trials of the NAOF task, which induced no adaptation, the AOF task rapidly induced complete adaptation; the subjects almost instantaneously became able to hit the target accurately (boxed in Fig. 2*G*). This is in contrast to the AOF-induced fast adaptation tested in the same subjects (Fig. 2*H*) ($P < 0.01$, Mann–Whitney *U* test; Fig. 2*I*). Apparently, learning proceeded during repeated trials of the NAOF task. This form of covert learning occurred during the NAOF task but not during the NF task (Fig. 2*J*).

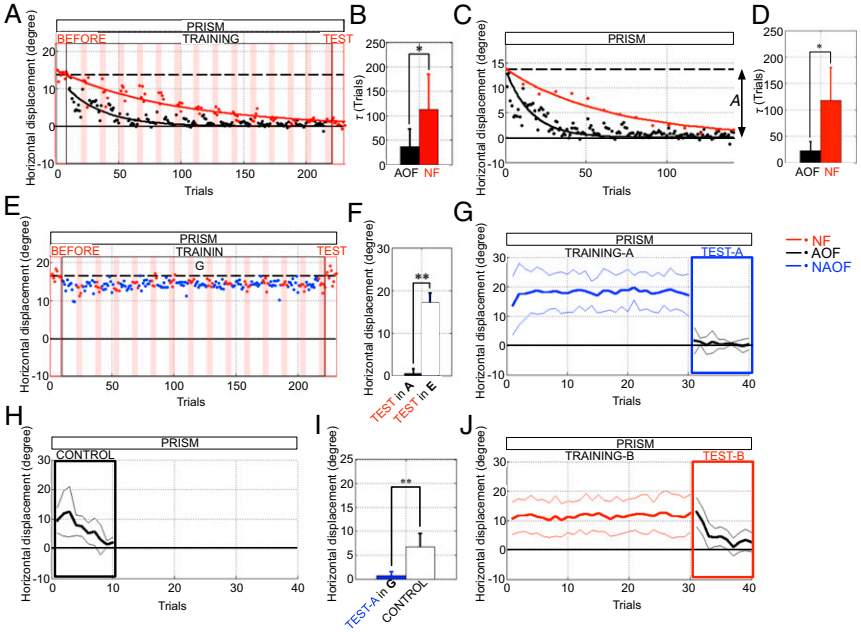

Fig. 2. Task-dependent fast and slow adaptation and hidden learning in healthy subjects. (*A*) Adaptation curves obtained by alternations between AOF phase (black dots, 10 trials, fast adaptation) and NF phase (red dots, five trials, slow adaptation). The dashed line indicates the baseline for the adaptive decreases in the degree of horizontal displacements. Red and black lines show fitted exponential curves. (*B*) Mean and SD of decay time constant of fitted curves for fast and slow adaptations. (*C*) Fast (black dots) and slow (red dots) adaptations determined by calculating averages during each NF trial. (*D*) Mean and SD of decay time constant of fitted curves for fast and slow adaptations determined by calculating averages during each NF trial. (*E*) Alternations between NAOF (blue dots, 10 trials) and NF (red dots 5, trials) tasks. (*F*) Horizontal displacements in TEST blocks in *A* and *E*. (*G*) Thirty trials of the NAOF task (blue lines, TRAINING session) followed by 10 trials of the AOF task [black lines, TEST-A session (box)]. (*H*) Test using the AOF task immediately after wearing a prism [CONTROL session (box)]. (*I*) Horizontal displacements in the AOF task in *G* (TEST-A block) and *H* (CONTROL block). (*J*) As in *G* but for the NF task (red lines). *$P < 0.05$ and **$P < 0.01$ by Mann–Whitney *U* test.

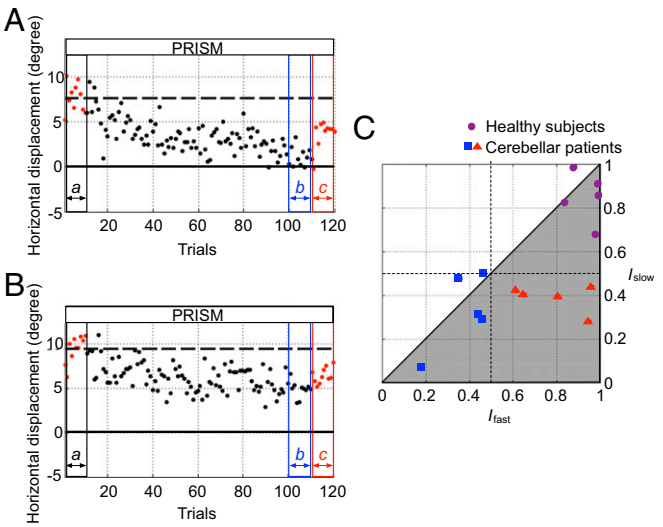

Fig. 3. Changes in internal model properties in cerebellar patients. (*A* and *B*) Averaged adaptation curves for cerebellar patients with spinocerebellar ataxia type 6 (SCA6) and spinocerebellar ataxia type 31 (SCA31) indicating I_{slow} <0.5 and I_{fast} ≥0.5 (Dis 1–5 in *SI Appendix*, Table S2) (*A*) or I_{slow} <0.5 and I_{fast} <0.5 (Dis 6–10 in *SI Appendix*, Table S2) (*B*). *a*, *b*, and *c* show the periods of 10 trials. (*C*) Scatter diagram of I_{fast} vs. I_{slow} for healthy subjects and cerebellar patients.

Computational Model for Motor Learning via Tandem Internal Models. We elaborated the tandem system (*SI Appendix*, Fig. S1) on the basis of currently available structural and functional knowledge of the hand-reaching system (Fig. 4*A*) as an internal model-based control system (9). The motor cortex acts as the controller of the right index finger to reach for a target (10). The controlled object involves a segmental circuit and a motor apparatus. A part of the cerebellum functioning as the forward model receives motor commands from the motor cortex via cerebellar mossy fibers and feeds back its output to the motor cortex. This circuit is mediated by the classic cerebrocerebellar communication loop (11). The forward model thus provides the motor cortex with an internal feedback loop that replaces an external feedback, as suggested early by Ito (1). Another area of the cerebellum is connected in parallel to the motor cortex via mossy fibers and functions as an inverse model (see ref. 12).

We further postulate the following. The prism plate adds an extra input (P in Fig. 4*A*) to the instruction signal to reach for the target position (x in Fig. 4*A*). The motor cortex is driven by the sum of x and P. The index finger's position [$y_{fast}(t, x)$ in Fig. 4*A* or $y_{slow}(t, x)$ in Fig. 4*B* at the tth trial] is determined by the sum of motor commands from the motor cortex in the internal feedback circuit (Z_M in Fig. 4*A*) and the inverse model in the feedforward circuit (Z_I in Fig. 4*A*). Furthermore, we postulated three types of instruction to the motor cortex (Fig. 4*A*). Instruction 1 (Ins 1) represents positions of the target point before reaching ($x + P$). This information is converted in the motor cortex into motor error (M_e), which activates learning processes in the inverse model via climbing fibers (Fig. 4*A*) (2). Instruction 2 (Ins 2) represents visual error signals (V_e), which activate learning processes in both the forward and inverse models via climbing fibers in the cerebellum (for review, see ref. 13). Instruction 3 (Ins 3) is generated from a high center and mediates the psychophysical command, "Do not learn from either motor or visual errors in determining the index finger's position." To execute this command, Ins 3 may block Ins 1 and Ins 2. This process is represented conveniently by switching off the circuit mediating Ins 1 and Ins 2 to the motor cortex (Fig. 4*C*).

The tandem system elaborated in Fig. 4*A* may operate as follows. In the AOF task, the gain of the forward model (G_F in Fig. 4*A*) is updated by learning from the visual error in hitting the target (V_e in Fig. 4*A*). The internal feedback via the updated forward model in turn alters the motor commands issued from the motor cortex. Motor errors (M_e in Fig. 4*A*) contained in the motor commands will then update the gain of the inverse model (G_I in Fig. 4*A*), as proposed by Kawato and Gomi (12). Thus, in the AOF task, both the forward and inverse models are updated, and their sum accounts for the fast adaptation [*SI Appendix*, Eq. **S4** in *SI Appendix*, *SI Text 3*].

In the NF task, in contrast, neither the forward model nor the inverse model is updated because of the absence of visual errors (Fig. 4*B*). This is consistent with the observation in the NF task that no adaptation occurred in hand-reaching movements (Fig. 1*D*). In the NAOF task, on the other hand, Ins 3 blocks the circuit that conveys motor and visual errors to the inverse model via the motor cortex (Fig. 4*C*); hence, updating occurring in the forward model cannot be transferred to the inverse model. This may be why, in the NAOF task, adaptation covertly occurs in the forward model, whereas no adaptation is induced in hand-reaching movements (Fig. 2*G*).

Normally, hand-reaching movements are performed by the parallel operation of two controller structures: the motor cortex associated with the forward model (green in Fig. 4*A*) and the inverse model (red in Fig. 4*A*). In the NF task, the motor cortex does not operate in hand reaching in the absence of visual errors; hence, hand-reaching movements are performed solely on the basis of the inverse model by feedforward control (Fig. 4*B*). Even in the presence of visual errors in the NAOF task, the switching-off by Ins 3 blocks the hand-reaching activity in the motor cortex, so that hand-reaching movements should be performed solely on the basis of the inverse model by feedforward control (red in Fig. 4*C*). These postulates are consistent with the absence of adaptation in hand-reaching movements in either the NF or NAOF task (Fig. 2*E*).

Finally, note that the slow adaptation occurred during the NF task alternating with the AOF task (Fig. 2*A*), whereas it did not occur during the NF task alone (Fig. 1*D*). This is because the inverse model is updated during the AOF task but not during the NF task.

Forward and Inverse Models in Adaptation. In Fig. 2*C*, the magnitude of horizontal deviations of hand reaching is plotted against trial number and fitted to exponential curves by the least squares

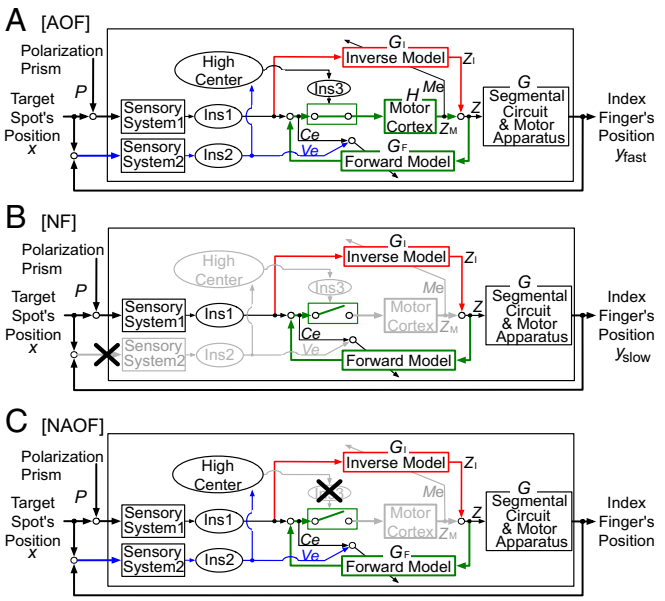

Fig. 4. Three types of learning operation in prism adaptation. Control system models for AOF (*A*), NF (*B*), and NAOF (*C*). **X** indicates the blockade of connection. The switch is operated by Ins3 (on in *A* and off in *B* and *C*). Red lines represent the feedforward circuit including the inverse model. Green lines represent the internal feedback circuit including the forward model. *Ce*, control error.

method. These exponential curves are redrawn in Fig. 5*A* in terms of the strength of adaptation measured from the zero baseline drawn at the starting point of the AOF task (dashed line in Fig. 2*C*). The strength of slow adaptation [$S_{slow}(t)$] is represented by a red line in Fig. 5*A*. The strength of fast adaptation [$S_{fast}(t)$] is represented similarly by a black line in Fig. 5*A*. Because the component including the inverse model is represented by the curve $S_{slow}(t)$ (red line in Fig. 5*A*), the other component including the forward model can be derived as $S_{diff}(t)$, the difference in strength between $S_{fast}(t)$ and $S_{slow}(t)$ [$S_{diff}(t) = S_{fast}(t) - S_{slow}(t)$] (green line in Fig. 5*A*). Whereas $S_{slow}(t)$ monotonically increased (*SI Appendix*, Eq. **S17**), $S_{diff}(t)$ increased across the initial 29 trials and then gradually decreased toward zero (*SI Appendix*, Eq. **S18**). Fig. 5*B* shows an area graph of relative adaptation strengths calculated using the data in Fig. 5*A*. The figure shows that, initially, the strength of adaptation in the forward model [$S_{diff}(t)$] predominates relative to the strength of adaptation in the inverse model [$S_{slow}(t)$], but the strengths become balanced at 50% each at the 40th trial and then are reversed, with the strength in the inverse model predominating. Hence, we can determine the relative strength and time courses of adaptive changes occurring in the forward and inverse models separately.

We derived the input–output relationship of the entire hand-reaching control system in a relatively simple form as an experimental formulation (*SI Appendix*, Eq. **S5**). With further calculation, we derived the gains and the time course of updating of the forward model (G_F) and inverse model (G_I) as functions of t and x (*SI Appendix*, Eqs. **S6** and **S8**). *SI Appendix*, Fig. S3*A* shows that when the subject is wearing the prism plate in the AOF task, the forward model gain increases rapidly and remains high, whereas the inverse model gain decreases slowly until a constant low gain is reached.

Patients with Cerebellar Neurodegeneration Show Selective Defects in Internal Models. In 10 patients with cerebellar diseases (*SI Appendix*, Table S2), various degrees of impairment in adaptation were observed, as exemplified in Fig. 3*A* (Dis 1–5) and Fig. 3*B* (Dis 6–10) in comparison with five healthy subjects (*SI Appendix*, Fig. S2 *A* and *B*). In the scatter diagram of the slow adaptation index [I_{slow}; 1 − (hand-reaching errors during period *c*)/(hand-reaching errors during period *a*)] vs. the fast adaptation index [I_{fast}; 1 − (hand-reaching errors during period *b*)/(hand-reaching errors during period *a*)] in Fig. 3*C*, we distinguish three types of pattern. In the first type, observed in the five healthy subjects, both I_{slow} and I_{fast} were high (>0.5), as indicated by purple circles in Fig. 3*C*. In the second type observed in five cerebellar patients (red triangles in Fig. 3*C*), I_{slow} was low (<0.5), suggesting an impaired inverse model. In these patients with the second-type pattern, the I_{fast} was high (>0.5), implying that the forward model remains normal and compensates for the impairment of the inverse model (*SI Appendix*, Fig. S3 *B*, *C*, and *E*). In the third pattern type observed in five other cerebellar patients, both I_{slow} and I_{fast} were low (<0.5) (blue squares in Fig. 3*C*), suggesting that both the forward and inverse models were impaired in these patients. Note in Fig. 3*C* that all these symbols fall within the triangular area representing $I_{slow} \leq I_{fast}$. This relationship can be derived theoretically (*SI Appendix*, Eq. **S23** in *SI Appendix*, *SI Text 5*), and it predicts that no patients show a high I_{slow} (similar to the normal inverse model) and a low I_{fast} (similar to the impaired forward model) (*SI Appendix*, *SI Text 1* and Fig. S3*C*).

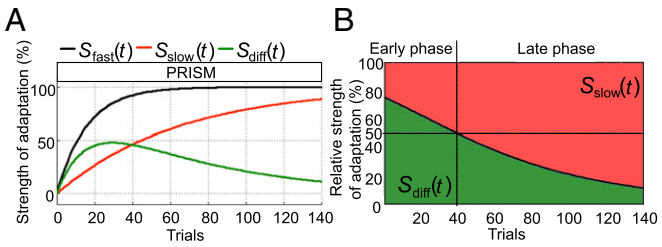

Fig. 5. Trial-based changes in strength of adaptation. (*A*) Strength of adaptation for each internal mode, derived from the inverse model [$S_{slow}(t)$, red line], motor cortex [$S_{diff}(t) = S_{fast}(t) - S_{slow}(t)$, green line], and total [$S_{fast}(t)$, black line] (Fig. 4*A*). These curves are estimated from Fig. 2*C*. (*B*) Area graph showing trial-dependent changes in the relative strength of adaptation in forward and inverse models. The black line shows [1 − $S_{slow}(t)$/$S_{fast}(t)$] × 100 based on the experimental results shown in Fig. 2*C*. Green and red areas indicate the ratios of the strengths of adaptation in the inverse model [$S_{slow}(t)$] and the forward model [$S_{diff}(t)$], respectively. $S_{diff}(t)$ is higher than $S_{slow}(t)$ during the initial 40 trials and decreases during the later trials.

Discussion

In this study, we observed the dynamic updating of motor learning in the prism-adaptation task, which could be explained computationally by a tandem system of forward and inverse models (*SI Appendix*, Eq. **S5**). The tandem system predicted three classes of subject responses—those with normal forward and inverse models, those with normal forward and impaired inverse models, and those with impaired forward and inverse models—which we validated in healthy subjects and patients with cerebellar degeneration.

Forward Versus Inverse Models in Motor Adaptation. In the historical literature, two types of internal model have been proposed. The idea of the forward model emerged from the interpretation of the cerebrocerebellar communication loop as a form of internal feedback (14, 15). In contrast, the inverse model is based on an open-loop feedforward control system (2). In studies of voluntary movement control, support for the operation of inverse models (e.g., refs. 10 and 16–18) or forward models (e.g., refs. 3, 19, and 20) has been largely presented without considering both models operating in coordination. In some studies, complex combinations of forward and inverse models have been proposed for some control tasks (e.g., refs. 5, 6, and 21), but the existence of such tandem systems was not computationally explored or experimentally validated.

There is an ongoing debate about which type of internal model, forward or inverse, is actually implemented in the cerebellum (22–25). A recent review of experimental data on various types of motor control indicated that either type of internal model operates, depending on available error information (for review, see ref. 13). In the present study, both types of internal model are assumed to be connected to the motor cortex in a tandem format and to assist hand reaching under various feedback conditions and executive instructions (*SI Appendix*, Fig. S1). In this tandem system, the forward and inverse models are updated differently in strength and trial number in prism adaptation (Fig. 5 and *SI Appendix*, Fig. S3*A*). Our results suggest that both forward and inverse models contribute to motor learning but do so in different ways. A recent experiment of monkey unit-recording showed that end-point error signals in the reaching experiment pass through motor cortices to the cerebellum via climbing fibers, corresponding to error in motor commands (M_e) in Fig. 4*A* (*SI Appendix*, *SI Text 2*) (10).

Our tandem model is composed by superposing Kawato et al.'s inverse model (2) and Ito's forward model (1). In our tandem model, the forward model is updated before the inverse model, allowing the solution to a one-to-many mapping problem by the inverse model (*SI Appendix*, *SI Text 4*) (26, 27).

Early and Late Phases of Prism Adaptation. In curves of responses to force field perturbation (28) and prism adaptation (29), fast and slow systems have been distinguished by fitting analysis and were considered to emerge from two different mechanisms. In contrast, our findings suggest that slow adaptation is hidden within fast adaptation on the basis of cerebellar motor learning (Fig. 5*A*). Previous studies also distinguished two phases in prism adaptation of hand reaching (30, 31). In the early phase, healthy subjects strategically and consciously control their hand movements to hit the aimed target precisely, and they recalibrate their spatial maps in the late phase. An fMRI study showed that these phases

are strongly related to blood oxygenation level-dependent (BOLD) activity in the cerebellum (32). Apparently, the initial peak of $S_{diff}(t)$ and the later increase in $S_{slow}(t)$ correspond to the early and late phases, respectively (Fig. 5*A*). In this study, we also noted the participants' common feeling that hand reaching at the beginning requires conscious effort but becomes more automatic as trials are repeated, in agreement with the tandem nature of internal models. Taken together, our findings provide an integrated framework for understanding a simple form of motor learning by a tandem combination of forward and inverse models with functional and anatomical specificities. The results suggest that in more complex motor behaviors multiplexed internal models may underlie computational structure learning, at least in the cerebellum.

Modeling Prism Adaptation. Prism adaptation has been examined using several different protocols involving dart or ball throwing or hand reaching (e.g., refs. 8 and 33). In these protocols, the magnitude of error (i.e., the actual deviation from the target) decreases rapidly during successive trials. In previous studies, the decay time (τ) of error determined by fitting with a simple exponential curve was used for evaluating dart-throwing adaptation (8, 34). Alternatively, the magnitude of reaching errors within the initial or first few trials after removing the prism was used to evaluate dart or ball throwing (8, 35–37) and hand-reaching (33, 38, 39) adaptations. The linear parametric model fits the adaptation curve in prism adaptation (40). A statistical model based on the Bayesian theory implied that state estimation using the forward model is important for prism adaptation (41). Recently, the hypothesis that motor learning consists of slow and fast systems (28) has been supported by prism adaptation (29). Our results support computational mechanisms of prism adaptation using the tandem system of the multiplexed forward and inverse models. Importantly, we determined the theoretical framework representing the characteristics of the tandem system involving both forward and inverse models (*SI Appendix*, Eqs. **S5** and **S6**).

Toward a Model-Based Clinical Index for Cerebellar Diseases. Neurological data support the hypothesis of the internal model (42), and several parameters have been proposed to reflect the motor-learning capability of patients with cerebellar disease (e.g., refs. 8 and 34). Previously, we defined an adaptability index (*AI*) which reflects the acquisition, retention, and extinction of prism adaptation and discriminates between patients with cerebellar diseases and healthy subjects (7). However, hand reaching had to be repeated in more than 200 trials. It is advantageous that we need only 120 trials to estimate I_{fast} and I_{slow} (Fig. 3 *A* and *B* and *SI Appendix*, Fig. S2*A*). These indices indicate the type of internal model that is impaired (Fig. 3*C*). We categorized the subjects into three types (Fig. 3*C* and *SI Appendix*, Table S3). There were no significant differences in age, disease type, and the scale for the assessment and rating of ataxia (SARA) between cerebellar patients with an impaired forward model and cerebellar patients with an impaired inverse model. I_{fast} and I_{slow} may serve as helpful measures in the medical diagnosis of cerebellar degeneration patients.

Neural Substrates Involved in Prism-Adaptation Effect. Monkey lesion and pharmacological inactivation studies (38, 43) along with human PET and fMRI studies (32, 44–47) have suggested the general involvement of the cerebellar cortex in the prism-adaptation task. Diedrichsen et al. (48) suggested on the basis of their human fMRI study that hand-reaching error signals are encoded in cerebellar lobules V, VI, and VIII and the dentate nucleus. Moreover, a recent study by Küper et al. (32) has suggested the involvement of cerebellar lobules VIII and IX and the dentate nucleus in the early phase of adaptation. In the late phase of adaptation, cerebellar lobules IV–VI are activated (32, 46, 49). A monkey unit-recording study also suggested that complex spikes from Purkinje cells in cerebellar hemispheric lobules IV–VI encode hand-reaching error signals (50). Taken together, these previous and our present findings suggest that the forward and inverse models are stored in lobules VIII–IX and lobules IV–VI, respectively.

Behavioral Instructions and Neural Responses. In the present study, we propose a challenging hypothesis that the psychophysical command to intentionally block the offline visual feedback is executed by signals sent from a high center to the motor cortex. These signals may switch off Ins 2 and 3 inputs to the motor cortex or suppress hand reaching-related activities in the motor cortex (Fig. 4 *B* and *C*). fMRI studies of humans revealed the decrease in the neuronal activity in the motor cortex evoked by repetitive peripheral nerve stimulation. This phenomenon is called "repetition suppression" (51, 52). A similar reduction in cortical activity measured as BOLD responses was observed in the primary motor cortex during movement repetition (53). Such reduction of cortical activity might underlie the decrease in outputs to the motor cortex in the later part of the green curve in Fig. 5*A*, suggesting that the hand-reaching movements after training are determined by the feedforward control (Fig. 4 *B* and *C*). On the other hand, Inoue et al. (10) reported that neuronal activity in monkey M1 increased when feedback error signals were provided before training. This increase is consistent with the increase in outputs of the motor cortex in the early part of the green line in Fig. 5*A*. Presently, therefore, our working hypothesis is that hand-reaching–specific control activity in the motor cortex determines hand-reaching behavior; the activity is increased by Ins 1 and Ins 2 input signals to the motor cortex (as represented by switching on in Fig. 4*A*) but is decreased by signals of Ins 3 (by switching off).

Materials and Methods

Participants. We recruited 10 healthy subjects and 10 patients with cerebellar diseases for the present study (*SI Appendix*, Tables S1–S3). Subjects were from a heterogeneous sample of individuals; patients with cerebellar diseases had different ranges of etiologies and degrees of clinical impairment. All participants provided informed consent and were compensated for their time in accordance with the protocol and experiments approved by the Ethics Committee of Tokyo Medical and Dental University (no. 1209). Furthermore, we divided the 10 healthy subjects into two groups (groups I and II in *SI Appendix*, Table S1).

Apparatus. The experimental apparatus has been described by Hashimoto et al. (7) and is described here only briefly. The subjects wore goggles containing a Fresnel prism plate, which shifts the visual field by 25° to the right. An electrically controlled shutter screen was attached to the goggles to block vision when required. The subject initially touched his/her index finger to a custom-made button switch attached to his/her right earlobe; then a target (a white circle; radius, 15 mm) was presented on a touchscreen. When the subject released his/her index finger from his/her earlobe, the electrical shutter prevented the subject from seeing his/her hand and the target until the target was touched. Thus, the subject was allowed to correct his/her reaching movements on the basis of touching error, i.e., the horizontal displacement between the touched and target positions, only when the electrical shutter was reopened after the target had been touched. Visual reaching task software (Katano Tool Software) was used to control the task with a conventional Windows 7 personal computer.

Data Sampling. We defined one trial as a series of finger movements from releasing the button switch attached to the earlobe to touching the touchscreen and then returning to repush the button switch. We carried out three tasks: the AOF, NF, and NAOF tasks. In the AOF task, the subject was able to confirm the touching error when he/she touched the touchscreen. In the NF task, the electrical shutter prevented the subject from confirming the touching error when he/she touched the screen. In the NAOF task, although the subject was able to confirm the touching error, we instructed them not to try to touch the target correctly and to intentionally ignore the outcome of preceding trials. Retesting in individual subjects was performed after an interval of at least 1 wk.

The subjects in group I wore the prism plate and repeated 100 trials of the AOF task (Fig. 1*C*). The subjects in groups I and II repeated 10 trials of the NF task (Fig. 1*D*).

The subjects in group II wore the prism plate and repeated 10 trials of the NF task in the BEFORE session (Fig. 2*A*). After that, the subjects repeated 14 alternations between 10 trials of the AOF task and five trials of the NF task in the TRAINING session, performing 210 trials in total. Finally, the subjects repeated 10 trials of the NF task in the TEST session. The subjects in group II wore

the prism plate and repeated 10 trials of the NF task in the BEFORE session (Fig. 2*E*). Next, the subjects conducted 14 alternations between 10 trials of the NAOF task and five trials of the NF task in the TRAINING session. After that, the subjects repeated 10 trials of the NF task in the TEST session. The subjects in group II wore the prism plate and repeated 30 trials of the NAOF task (TRAINING-A) and then performed 10 trials of the AOF task (TEST-A in box, Fig. 2*G*). One week later, the same subjects again performed 10 trials of the AOF task (CONTROL in box, Fig. 2*H*). One month later, they performed 30 trials of the NF task (TRAINING-B, Fig. 2*H*) and then 10 trials of the AOF task (TEST-B in box, Fig. 2*J*). The patients with cerebellar diseases (Fig. 3 *A* and *B* and *SI Appendix*, Fig. S2 *C* and *D*) and healthy subjects in group I (*SI Appendix*, Fig. S2 *A* and *B*) performed 10 trials of the NF task (period *a*), 100 trials of the AOF task, and 10 trials of the NF task again (period *c*).

Data Analysis. We measured the magnitude of finger-touch errors (r) as the degree of horizontal displacement between the touch points and the center of the target on the touchscreen. The adaptation curves in the TRAINING session in Fig. 2 *A* and *C* were fitted as follows:

$$r = \eta \cdot \exp(-t/\tau), \quad [1]$$

where η is the magnitude of finger-touch error in the first trial of the TRAINING session, and t is the trial number from the start of the session. The time constant τ was defined as the number of trials taken in the session for the finger-touch error to approach 36.8%, e^{-1} of η, namely, the rate of decay of an exponential curve. The Mann–Whitney *U* test was utilized to examine the statistically significant differences in τ between fast and slow adaptations (Fig. 2 *A* and *C*) between horizontal displacements during the TEST sessions (Fig. 2 *A* and *E*) and between horizontal displacements during the TEST-A session (Fig. 2*G*) and the CONTROL session (Fig. 2*H*).

To these patients, as a minimum requirement, we administered the first 10 trials of the NF task (period *a*) to obtain their degree of horizontal displacement as the control, followed by 100 trials of the AOF task to induce fast adaptation and then another 10 trials of the same task to test the thus-induced fast adaptation (period *b*). Finally, 10 NF trials were administered (period *c*) to test the slow adaptation. We then measured the mean magnitude of hand-reaching errors during periods *a*, *b*, and *c* as D_a, D_b, and D_c, respectively. The fast adaption index I_{fast} is defined as $1 - (D_b/D_a)$, and the slow adaptation index I_{slow} is defined as $1 - (D_c/D_a)$. I_{slow} and I_{fast} are related to slow and fast adaptations, respectively, around the 110th trial (see details in *SI Appendix*, *SI Text 5*).

ACKNOWLEDGMENTS. We thank the healthy volunteers, patients, and their families for participation in this study; K. Katano (Katano Tool Software) for help with development of tools; M. Takano, A. Tanaka, H. Ibi, K. Soga, M. Nakao, K. Matsumura, and A. Honda for help with task support; and Dr. C. Yokoyama (RIKEN Brain Science Institute) for critical reading of the manuscript. This work was supported by Grants-in-Aid for Strategic Research Program for the Brain Sciences (Understanding of molecular and environmental bases for brain health) by the Ministry of Education, Culture Sports, Science and Technology of Japan, research funds from RIKEN, and Grant-in-Aid for Young Scientists (B) 16k21649.

1. Ito M (1970) Neurophysiological aspects of the cerebellar motor control system. *Int J Neurol* 7:162–176.
2. Kawato M, Furukawa K, Suzuki R (1987) A hierarchical neural-network model for control and learning of voluntary movement. *Biol Cybern* 57:169–185.
3. Wolpert DM, Miall RC (1996) Forward models for physiological motor control. *Neural Netw* 9:1265–1279.
4. Ito M, Yamaguchi K, Nagao S, Yamazaki T (2014) Long-term depression as a model of cerebellar plasticity. *Prog Brain Res* 210:1–30.
5. Wolpert DM, Kawato M (1998) Multiple paired forward and inverse models for motor control. *Neural Netw* 11:1317–1329.
6. Mischiati M, et al. (2015) Internal models direct dragonfly interception steering. *Nature* 517:333–338.
7. Hashimoto Y, et al. (2015) Quantitative evaluation of human cerebellum-dependent motor learning through prism adaptation of hand-reaching movement. *PLoS One* 10: e0119376.
8. Martin TA, Keating JG, Goodkin HP, Bastian AJ, Thach WT (1996) Throwing while looking through prisms. I. Focal olivocerebellar lesions impair adaptation. *Brain* 119:1183–1198.
9. Ito M (2012) *The Cerebellum: Brain for an Implicit Self* (FT, Upper Saddle River, NJ).
10. Inoue M, Uchimura M, Kitazawa S (2016) Error signals in motor cortices drive adaptation in reaching. *Neuron* 90:1114–1126.
11. Ramnani N (2006) The primate cortico-cerebellar system: Anatomy and function. *Nat Rev Neurosci* 7:511–522.
12. Kawato M, Gomi H (1992) A computational model of four regions of the cerebellum based on feedback-error learning. *Biol Cybern* 68:95–103.
13. Ito M (2013) Error detection and representation in the olivo-cerebellar system. *Front Neural Circuits* 7:1.
14. Dum RP, Strick PL (2003) An unfolded map of the cerebellar dentate nucleus and its projections to the cerebral cortex. *J Neurophysiol* 89:634–639.
15. Kelly RM, Strick PL (2003) Cerebellar loops with motor cortex and prefrontal cortex of a nonhuman primate. *J Neurosci* 23:8432–8444.
16. Imamizu H, et al. (2000) Human cerebellar activity reflecting an acquired internal model of a new tool. *Nature* 403:192–195.
17. Gomi H, Kawato (1996) Equilibrium-point control hypothesis examined by measured arm stiffness during multijoint movement. *Science* 272:117–120.
18. Takamuku S, Gomi H (2015) What you feel is what you see: Inverse dynamics estimation underlies the resistive sensation of a delayed cursor. *Proc Biol Sci* 282:20150864.
19. Izawa J, Criscimagna-Hemminger SE, Shadmehr R (2012) Cerebellar contributions to reach adaptation and learning sensory consequences of action. *J Neurosci* 32:4230–4239.
20. Diedrichsen J, Verstynen T, Hon A, Zhang Y, Ivry RB (2007) Illusions of force perception: The role of sensori-motor predictions, visual information, and motor errors. *J Neurophysiol* 97:3305–3313.
21. Wagner MJ, Smith MA (2008) Shared internal models for feedforward and feedback control. *J Neurosci* 28:10663–10673.
22. Kobayashi Y, et al. (1998) Temporal firing patterns of Purkinje cells in the cerebellar ventral paraflocculus during ocular following responses in monkeys II. Complex spikes. *J Neurophysiol* 80:832–848.
23. Winkelman B, Frens M (2006) Motor coding in floccular climbing fibers. *J Neurophysiol* 95:2342–2351.
24. Ebner TJ, Pasalar S (2008) Cerebellum predicts the future motor state. *Cerebellum* 7: 583–588.
25. Ebner TJ, Hewitt AL, Popa LS (2011) What features of limb movements are encoded in the discharge of cerebellar neurons? *Cerebellum* 10:683–693.
26. Poggio T, Girosi F (1990) Regularization algorithms for learning that are equivalent to multilayer networks. *Science* 247:978–982.
27. Schenck W (2011) Kinematic motor learning. *Connect Sci* 23:239–283.
28. Smith MA, Ghazizadeh A, Shadmehr R (2006) Interacting adaptive processes with different timescales underlie short-term motor learning. *PLoS Biol* 4:e179.
29. Inoue M, et al. (2015) Three timescales in prism adaptation. *J Neurophysiol* 113:328–338.
30. Redding GM, Wallace B (1996) Adaptive spatial alignment and strategic perceptual-motor control. *J Exp Psychol Hum Percept Perform* 22:379–394.
31. Redding GM, Rossetti Y, Wallace B (2005) Applications of prism adaptation: A tutorial in theory and method. *Neurosci Biobehav Rev* 29:431–444.
32. Küper M, et al. (2014) Activation of the cerebellar cortex and the dentate nucleus in a prism adaptation fMRI study. *Hum Brain Mapp* 35:1574–1586.
33. Weiner MJ, Hallett M, Funkenstein HH (1983) Adaptation to lateral displacement of vision in patients with lesions of the central nervous system. *Neurology* 33:766–772.
34. Thach WT, Goodkin HP, Keating JG (1992) The cerebellum and the adaptive coordination of movement. *Annu Rev Neurosci* 15:403–442.
35. Fernández-Ruiz J, Díaz R (1999) Prism adaptation and aftereffect: Specifying the properties of a procedural memory system. *Learn Mem* 6:47–53.
36. Block HJ, Bastian AJ (2012) Cerebellar involvement in motor but not sensory adaptation. *Neuropsychologia* 50:1766–1775.
37. Gutierrez-Garralda JM, et al. (2013) The effect of Parkinson's disease and Huntington's disease on human visuomotor learning. *Eur J Neurosci* 38:2933–2940.
38. Baizer JS, Kralj-Hans I, Glickstein M (1999) Cerebellar lesions and prism adaptation in macaque monkeys. *J Neurophysiol* 81:1960–1965.
39. Tseng YW, Diedrichsen J, Krakauer JW, Shadmehr R, Bastian AJ (2007) Sensory prediction errors drive cerebellum-dependent adaptation of reaching. *J Neurophysiol* 98:54–62.
40. Kitazawa S, Kohno T, Uka T (1995) Effects of delayed visual information on the rate and amount of prism adaptation in the human. *J Neurosci* 15:7644–7652.
41. Yamamoto M, Ando H (2012) Probabilistic models of state estimation predict visuomotor transformations during prism adaptation. *Vis Neurosci* 29:119–129.
42. Manto M (2009) Mechanisms of human cerebellar dysmetria: Experimental evidence and current conceptual bases. *J Neuroeng Rehabil* 6:10.
43. Norris SA, Hathaway EN, Taylor JA, Thach WT (2011) Cerebellar inactivation impairs memory of learned prism gaze-reach calibrations. *J Neurophysiol* 105:2248–2259.
44. Clower DM, et al. (1996) Role of posterior parietal cortex in the recalibration of visually guided reaching. *Nature* 383:618–621.
45. Danckert J, Ferber S, Goodale MA (2008) Direct effects of prismatic lenses on visuomotor control: An event-related functional MRI study. *Eur J Neurosci* 28:1696–1704.
46. Luauté J, et al. (2009) Dynamic changes in brain activity during prism adaptation. *J Neurosci* 29:169–178.
47. Chapman HL, et al. (2010) Neural mechanisms underlying spatial realignment during adaptation to optical wedge prisms. *Neuropsychologia* 48:2595–2601.
48. Diedrichsen J, Hashambhoy Y, Rane T, Shadmehr R (2005) Neural correlates of reach errors. *J Neurosci* 25:9919–9931.
49. Donchin O, et al. (2012) Cerebellar regions involved in adaptation to force field and visuomotor perturbation. *J Neurophysiol* 107:134–147.
50. Kitazawa S, Kimura T, Yin PB (1998) Cerebellar complex spikes encode both destinations and errors in arm movements. *Nature* 392:494–497.
51. Poldrack RA (2000) Imaging brain plasticity: Conceptual and methodological issues–A theoretical review. *Neuroimage* 12:1–13.
52. Grill-Spector K, Henson R, Martin A (2006) Repetition and the brain: Neural models of stimulus-specific effects. *Trends Cogn Sci* 10:14–23.
53. Hamilton AF, Grafton ST (2009) Repetition suppression for performed hand gestures revealed by fMRI. *Hum Brain Mapp* 30:2898–2906.